Experimental Study on High-Cycle Fatigue Properties of Q420C Steel at Room Temperature

Liguo Yang[a,b] 🆔 *, Yongming Xing[b*]*

[a]Inner Mongolia University of Technology, School of Civil Engineering, Hohhot, 010051, China.
[b]Inner Mongolia University of Technology, School of Science, Hohhot, 010051, China.

Q420 structural steel, which is widely used in transmission towers and offshore platform structures, has been studied less than other steels. However, fatigue failure of offshore platform structures can occur under repeated wave loads. The fatigue strength applied stress–number of cycles (S-N) curves of Q420C structural steel were obtained by performing static tensile tests and high-cycle fatigue tests, and the fatigue crack formation and development were investigated based on the fracture morphology. The steel fatigue lifetimes were compared with standard curves and those of steels with various strengths reported previously. The results showed that the fatigue failure of the specimen was typical, and the fracture surface could be divided into a crack initiation region, a propagation region, and a transient fracture region. The Q420C curve was above the BS7608:2014, GB50017-2017, and ANSI/AISC360-10 standard curves. The S-N curve specified in the standard is conservative for Q420C steel. The strength of the steel directly affected its fatigue properties, and the thickness of the steel plate had a significant effect on the fatigue properties.

Keywords: *High-cycle fatigue, fatigue strength, fatigue damage, S-N curve.*

1. Introduction

Q420 steel is a low-alloy and high-strength-structural steel produced in China through a microalloying and hot mechanical rolling process. It has high comprehensive mechanical properties and is mainly used in transmission towers, offshore platform structures, oil derricks, and coal mine steel structural supports[1]. For example, with an offshore platform structure, fatigue failure of the structure can easily occur under long-term repeated wave loads. The fatigue failure of the steel and its joints has become the focus of structural engineers.

There have been many studies on the high-cycle fatigue properties of various steels, which mainly determined the applied stress-number of cycles (S-N) relationships through traditional fatigue tests and data fitting. Shi et al.[2-4] conducted room-temperature high-cycle fatigue tests on Q390GJD, Q460C, and Q460D steel under a loading frequency of 105 Hz, fitted the fatigue life S-N curves of the three kinds of steel, and determined that the values of the probabilistic stress life (P-S-N) curves and 95% guarantee rate of Q390GJD and Q460D steels were much higher than those in the GB50017-2003 standard. The values of the P-S-N curves and 95% guarantee rate in Q460D steel tests were basically consistent with the calculated values in the GB50017-2003 standard. The discrepancies of the steel fatigue tests were caused by the geometric parameters of the fatigue specimens and material defects. Kang and Hong[5] conducted an experimental study on the high-cycle fatigue performances of 10-mm-thick Q690D high-strength steel plates and fitted the S-N curves. The fitting results showed that the fatigue performances of Q690D high-strength steel

was superior. Compared with the existing fatigue test curves and standard fatigue curves of other strength grades of steel, it was concluded that the fatigue performance of various steels is highly related to the yield strength, and the calculated values based on the standard curve are conservative. Tong et al.[6] tested and studied the mechanical properties and fatigue properties of four kinds of high-strength structural steels (Q460, Q550, Q690, and Q960). Tensile tests showed that with the increase in the yield strength, the size of the yield platform decreased gradually, and the yield ratio increased significantly. High-cycle fatigue tests showed that the fatigue strength of steel increased significantly with the increase in the yield strength, and the values were significantly higher than those in the current standard. Moreover, the increase in the fatigue strength lagged behind that of the static strength. Guo et al.[7-10] introduced a theoretical method for calculating the fatigue life by summarizing the research status of the fatigue properties of high-strength steel. According to the fatigue test data of Q460D, Q690D, and other high-strength steels, the development of the fatigue lives of high-strength steels was analyzed, and the fatigue resistances of high-strength steels were evaluated with different fatigue design codes. The results showed that the fatigue performance of the high-strength steel was better than that of ordinary steel, and the standard design curves underestimated the fatigue performance of high-strength steel.

Fan[11] verified the feasibility of fatigue thermography tests by comparing the traditional high-cycle fatigue tests and fatigue thermography tests of Q235 steel. Based on the energy dissipation caused by deformation, a calculation model of the energy dissipation was established, and combined with thermal image data, the fatigue lives of materials were predicted quickly. Liu et al.[12,13] obtained the S-N curve of the fatigue stress life of Q345 steel under different failure

probabilities through high-cycle fatigue tests. Additionally, the temperature field on the sample surface was recorded by an infrared thermal imager. It was concluded that there was a nonlinear relationship between the inherent dissipative energy of a unit volume of the material and the load, and the characterization model of the inherent dissipative energy of the unit volume material was established in the framework of thermodynamics. Cicero et al.[14] carried out high-cycle fatigue tests on various structural steels (S355M, S460M, S690Q, and S890Q) under three hot cutting methods (oxygen, plasma, and laser cutting), obtained the high-cycle fatigue strength S-N curves, and aligned them with the fatigue design grade in the corresponding bs7608 design standard. Finally, a large number of experimental data in the literature were compared and verified. Zhang et al.[15] conducted high-cycle fatigue tests on Q420B steel at four temperatures (25°C, 0°C, −15°C, and −30°C) with three stress amplitudes ($0.5f_y$, $0.7f_y$, and $0.9f_y$). The research showed that when the stress amplitude was $0.5f_y$, the base metal sample did not exhibit fatigue fracture or significant deformation at the four temperatures when the number of loading cycles exceeded two million. At the same stress level, the fatigue life of the base metal sample was significantly affected by the temperature changes, that is, a low temperature could improve the fatigue properties of Q420B steel.

To date, most of the research on fatigue strength of structural steel is on ordinary strength or high performance steel. However, the larger application range of intermediate strength Q420 steel and its connection fatigue strength test research is less. In this study, the tensile properties and room temperature fatigue properties of Q420C structural steel were experimentally investigated. The fatigue strength S-N curves were fitted to the trial records, the generation and extension of fatigue cracks were studied based on the fracture morphology, and the fatigue lives of the steel specimens were compared with that of reference and criterions. The relevant research results provided tentative data support for the fatigue strength analysis and life prediction of Q420C structural steel.

2. Uniaxial Tensile Tests

2.1. Experimental design

Q420C 8-mm-thick steel plate produced by a Chinese steel plant was used in this test, and the sample thickness was the full plate thickness. The steel plate met the demands of chinese product standard GB/T1591-2008[16]. Chemical components of Q420C steel plate are presented in Table 1. The product standard values in this table are the extreme values specified in GB/T1591-2008. The factory values were the measured values provided by the product factory certificate, and the measured values were the measured values from the melting analysis performed in this study. The factory and measured values met the GB/T1591-2008 requirements.

Static tensile tests were carried out according to chinese standard GB/T228.1-2010[17], so as to obtain the tensile mechanical properties of Q420C steel plate. The sample size is shown in Figure 1, and the sample length direction was the rolling direction of the steel plate. Three monotonic tensile specimens and 12 high-cycle fatigue test specimens were designed. The specimen details were presented in Table 2.

2.2. Tensile test results

According to the chinese standard GB/T228.1-2010, the monotonic static tensile tests were carried out. The loading mode was displacement control until the sample broke, and the loading rate was 0.4 mm/min and remains unchanged. The force-displacement curve of the sample obtained by monotonic static tension test are presented in Figure 2, and the results of test for each sample are shown in Table 3.

The failure position of the connecting specimen was near the arc transition section. From the tensile fracture surfaces, all the samples had typical elastoplastic deformation characteristics. Relative deviation in the breaking yields and ultimate loads of the three specimens were less than 5%, which showed that the steel material was uniform and the quality was stable. The average yield-strength ratio was
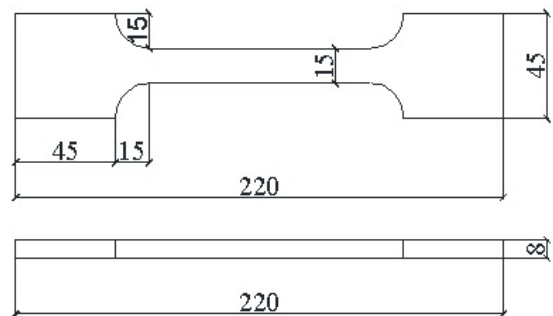

Figure 1. Sample size (mm).

Table 1. Chemical components of Q420C steel (%).

components	C	Si	Mn	Ni	Cr	Cu	Mo	B	V	C_{eq}
Measured values	0.14	0.042	0.8	0.007	0.015	0.017	0	-	0	0.278
Factory values	0.07	0.19	1.08	0.01	0.02	0.03	0.004	-	0	-
Product standard	≤0.20	≤0.50	≤1.7	≤0.80	≤0.30	≤0.30	≤0.20	-	≤0.20	≤0.48

Table 2. Sample grouping.

Specimen	Test classification	Subgroup	Number
Base metal	tensile test	MCD	3
	Fatigue test	MCX	12

0.87, which exceeded the requirement of the yield-strength ratio being less than or equal to 0.85 in the plastic design and seismic performance-based design of steel structures. The force-deformation curves of the specimens could be divided into four stages: elastic, yield, strengthening, and failure stages. However, the yield platforms of the specimens were shorter than that of plain carbon steel.

3. High-Cycle Tensile Fatigue Test

3.1. Fatigue strength theory

At present, the fatigue strength is evaluated or estimated mainly by establishing the relation between the applied load S and the material fatigue life cycle N, which is called Wöhler curve[18]. A complete S-N curve can be divided into three sections: a low-cycle fatigue region, a high-cycle fatigue region, and an ultra-high-cycle fatigue region. The S-N curve of the high-cycle fatigue region is almost a straight line in the logarithmic coordinate system, which is usually described by a power function or a logarithmic form:

$$S^m N = C \tag{1a}$$

$$\log S = A + B \log N \tag{1b}$$

where S is the section fatigue strength of the structure details, N is cycle number of the cyclic loading, m is the exponent of the S-N relation of the power function form, B is the gradient of the Miner's linear S-N regular, A and C are coefficients.

Since the development of fracture mechanics, the solutions of fatigue problems have provided new research means. According to linear elastic fracture mechanics, there is an initial crack a_0 in the structural material. With the increase in the stress cycle number, the initial defect expands. When the crack length reaches the critical value of a_{cr}, the structure fails. Paris proposed the following relationship between the rate of fatigue crack growth and the stress intensity factor increment ΔK[19]:

$$\frac{da}{dN} = f(\Delta K) = C(\Delta K)^n \tag{2}$$

The integral of (2) provides the following expression for the fatigue life:

$$N = \frac{1}{C} \int_{a_0}^{a_{cr}} \frac{da}{(\Delta K)^n} \tag{3}$$

where a_0 and a_{cr} are the initial crack size and the final crack size. ΔK is defined as the stress intensity factor increment, and $\Delta K = \alpha \sqrt{\pi a} \times \Delta \sigma$. where $\Delta \sigma$ is the stress variation range. The simplified form of (3) is as follows:

$$N = (\Delta \sigma)^{-n} \left[\frac{1}{C} \int_{a_0}^{a_{cr}} \frac{da}{(\alpha \sqrt{\pi a})^n} \right] \tag{4a}$$

$$N = \beta (\Delta \sigma)^{-n} \tag{4b}$$

In the above equations, $\beta = 2\left(C\pi^{3/2}\sqrt{a_0}\right)^{-1}$. Formulas 4a and 4b can be used to determine the extended fatigue life and residual strength.

3.2. Fatigue test results

Twelve fatigue loaded specimens of the MCX series were tested on an MTS fatigue testing machine. For the test, the chinese standard GB/T3075-2008 was followed[20]. The room temperature fatigue loading adopted the force control mode. The loading waveform was a sinusoidal, constant-amplitude, alternating waveform. The loading frequency was set to 10 Hz. The stress ratio was defined as $r = P_{min}/P_{max} = 0.1$. P_{max} was calculated based on kF_y, k is the loading factor, F_y is the yield point load of the sample under monotonic tension. The service load in a normal service state does not exceed $0.66F_y$[21], and the initial value of k was 0.7 times the yield load F_Y under monotonic tension. The value of k was varied until the number of stress cycles N reached two million without damage. The high-cycle fatigue tests of 12 specimens were carried out under 10 stress levels. The fatigue failure position of the connecting specimen was near the stress concentration area of the arc transition section. The test results for each sample are shown in Table 4.
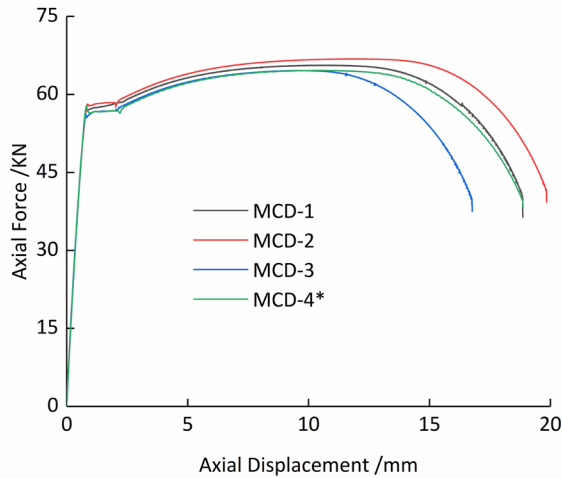

Figure 2. Monotonic tension load-displacement curves.

Table 3. Tensile test results.

Sample	F_y/kN	F_u/kN	f_y/MPa	f_u/MPa	F_y/F_u
MCD-1	57.4	65.6	478.3	546.7	0.87
MCD-2	58.0	66.8	483.3	556.7	0.87
MCD-3	56.8	64.5	473.3	537.5	0.88
average	57.4	65.6	478.3	546.7	0.87

Table 4. Fatigue test parameters and results of base material specimen.

Specimen number	k	P_{max}/KN	S_{max}/MPa	S/MPa	F/Hz	N
MCX-1	0.7	40.25	335.42	301.88	10	641,002
MCX-2	0.8	46	383.33	345.00	10	444,288
MCX-3	0.65	37.375	311.46	280.31	10	459,783
MCX-4	0.68	39.11	325.92	293.33	10	684,581
MCX-5	0.6	34.5	287.50	258.75	10	809,379
MCX-6	0.55	31.625	263.54	237.19	10	2,000,000
MCX-7	0.58	33.35	277.92	250.13	10	1,949,573
MCX-8	0.62	35.65	297.08	267.38	10	1,504,734
MCX-9	0.72	41.4	345.00	310.50	10	524,530
MCX-10	0.75	43.125	359.38	323.44	10	228,423
MCX-11	0.6	34.5	287.50	258.75	10	824,563
MCX-12	0.65	37.375	311.46	280.31	10	724,212
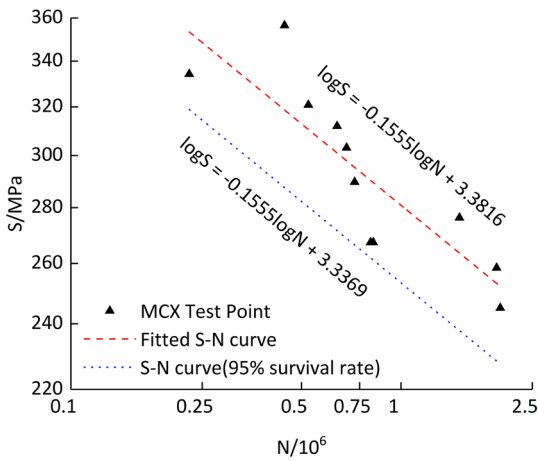
Figure 3. Fitted applied stress–number of cycles (S-N) curve in logarithmic coordinates.
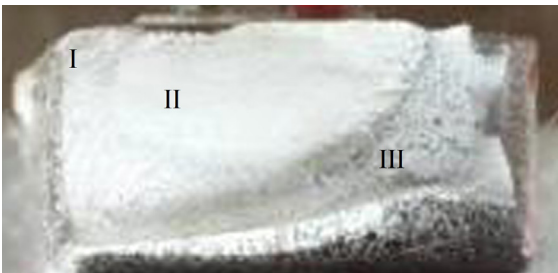
Figure 4. Macrofractography (MCX-5).

The MCX-3 data points deviated significantly from the others. This specimen underwent a large amount of initial bending before loading, which was eliminated in the analysis because the data were abnormal. With reference to Formula 1a, the test data were linearly fitted by the least squares method, and the fitting results are shown in Figure 3. The median S-N relationship of $\log S = -0.1555 \log N + 3.3816$ at the significance level of 0.05 was obtained, where S is the section fatigue strength of the applied load, N is cycle number of the cyclic loading, and the standard deviation SD

was 0.02716. The correlation coefficient r was 0.714, which met the requirement of the critical value, $r > r_a = 0.602$.

3.3. Fracture analysis

After the high-cycle fatigue test, the fracture section of the sample could be divided into three regions: fatigue crack initiation region I, stable extension region II and Instantaneous fracture region III. In this paper, the MCX-5 specimen was subjected to a stress of 287.50 MPa. The fatigue fracture surface is shown in Figure 4 after 809,379 cycles. The fracture surface had a typical fatigue fracture morphology. The fracture surfaces of the specimens were continuously opened, closed, and rubbed against each other before fatigue breaking, which resulted in flat and smooth fracture surfaces. The fracture surfaces were coarse and uneven, similar to those in the static strength experiments.

The fracture surface of the MCX-5 specimen was examined using a HitachiS-4800 scanning electron microscope. The microstructure was shown in Figure 5. Figure 5a shows the crack source region. At a 50× magnification, a similar inclusion defect was visible on and around the specimen, forming a local stress concentration and producing an initial microcrack. There were three types of fatigue crack growth mechanisms: the micro-cleavage type, the striation type, and the micropore aggregation type. Figure 5b shows the 500× magnification of the fracture zone. A typical fracture morphology, which included secondary cracks, fatigue striations, and microcleavage, was evident. Figure 5c shows the sample broken area at 1000× magnification. Dense dimples of different sizes were evident. It is not easy to slip between the dimples, highlighting the rapid extension of material damage.

3.4. Displacement analysis

The fatigue tests of the MCX series specimens were designed with two million failure cycles and two million continuous failure cycles. Figure 6 shows the relation between the displacement values and the recycle ratio for some specimens under the maximum load during fatigue loading. δ is the axial deformation of the sample under the maximum load, N is cycle number of the cyclic loading, and N_f is the fatigue life of the sample.
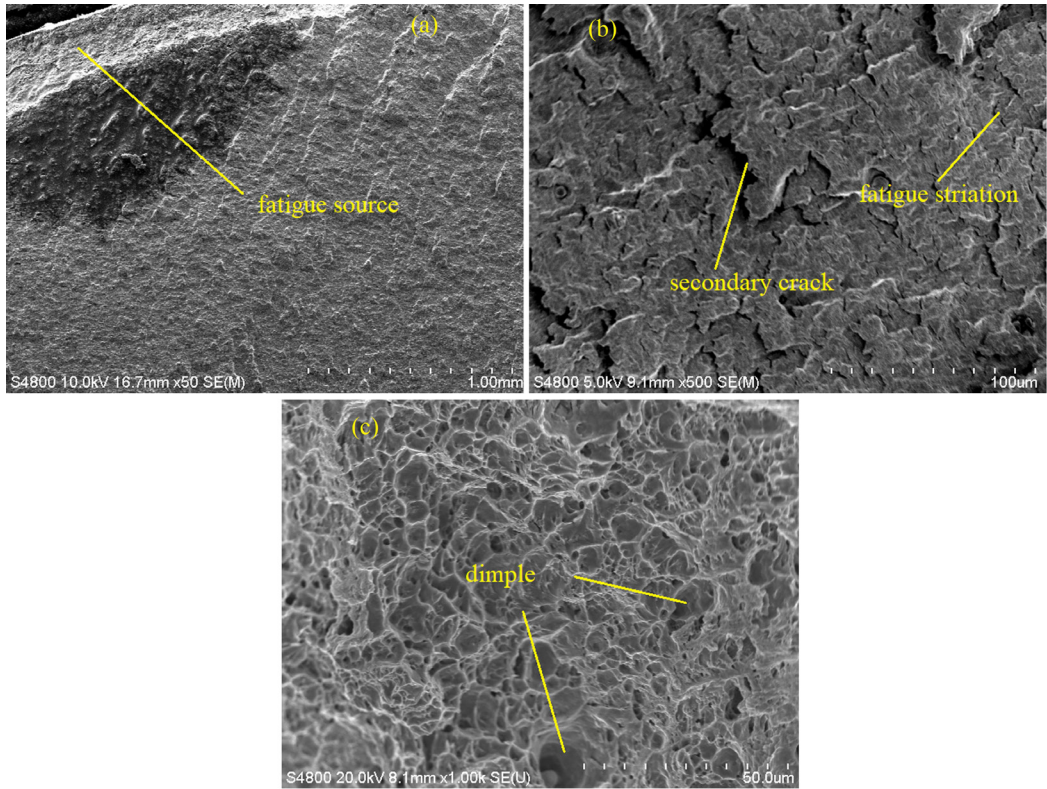
Figure 5. Microanalysis for fracture of base metal (MCX-5). (a) Crack initiation region, (b) Stable extension region, (c) Instantaneous fracture region.
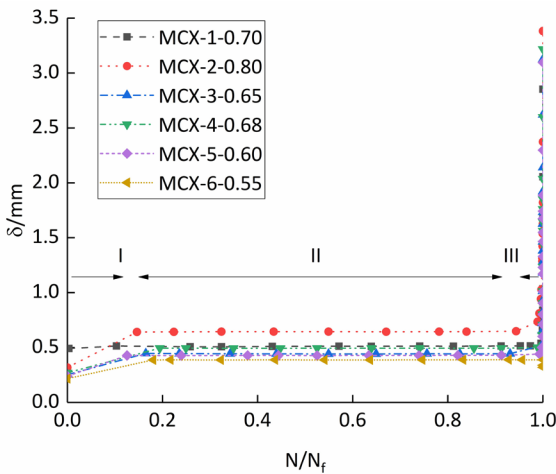

Figure 6. Fatigue displacement curve.

When the loading coefficient k = 0.55, the MCX-6 specimen was not broken after two million stress cycles, and the loading was stopped. During the fatigue loading process, the displacement value corresponding to the maximum load of the unbroken specimen was small, and the value corresponded to stages I and II in Figure 6. When the loading factor took other values, the test specimen underwent fatigue fracture in two million stress cycles. The variation of the fatigue displacement of the fracture

specimen with the loading cycle ratio corresponded to stages I, II, and III in Figure 6. Stage I was the stage in which the displacement was slowly increased. the recycle ratio N/N_F was less than 0.2. The crack originated from the persistent slip band, grain boundaries, inclusions, pores, and other defects on the surface. The micro-performance involved crack nucleation, plastic deformation recovery, and slip band formation, and the macro-performance involved the increase in the displacement under the maximum load. Stage II was the stage of stable deformation changes. Under the action of extreme stresses of 335.42, 383.33, 311.46, 325.92, 287.50, and 263.54 MPa, the corresponding fatigue deformations of the MCX series specimens were 0.51, 0.64, 0.44, 0.49, 0.42, and 0.38 mm, respectively. The deformations of the specimens were direct ratio relation with the applied force, and the maximum displacement remained unchanged. Stage III was a stage of rapid increase of the displacement. When the recycle ratio $N/N_F > 0.9$, the displacements of the specimen increased rapidly and broke, and the plastic deformation characteristics of the new fracture were remarkable. The change of the displacement under the maximum load could reflect the fatigue failure process.

3.5. Fatigue damage analysis

The damage of an engineering structure or mechanical connection is largely caused by the damage accumulation caused by the repeated and cyclic action of a load. Fatigue damage theory was established by the law of cumulative fatigue damage and the failure criterion to estimate the

remaining service lives of engineering structures under specific service conditions[18]. In this paper, under uniaxial tensile tests, the damage variable $D = 1/N_f$ in the process of a stress cycle was defined, and it remained unchanged. N_F was the fatigue life, and the damage caused by N cycles could be expressed as $D = N/N_f$. In the high-cycle fatigue test, in addition to the large plastic damage when the fatigue life was about to be reached, the plastic deformation in the whole loading process was very small, and the plastic cumulative strain rate was taken as 0. The damage model can be expressed as follows[22]:

$$\frac{dD}{dN} = \frac{2B\left(S_{max}^{\beta+1} - S_{min}^{\beta+1}\right)}{(\beta+1)(1-D)^{\beta+1}} \tag{5}$$

where S_{max} and S_{min} are the maximum cross section stress and minimum stress under the repeated loads, respectively. B and β are the fatigue strength constants of the material, it can be obtained through material fatigue tests. For the initial condition, when N = 0 and D = 0, the integral of Equation 5 can be obtained as follows:

$$\frac{1}{(\beta+2)}\left[1-(1-D)^{(\beta+2)}\right] = \frac{2B\left(S_{max}^{\beta+1} - S_{min}^{\beta+1}\right)}{(\beta+1)}N \tag{6}$$

Introducing the boundary conditions $N = N_F$ and D = 1, a transformation of Equation 6 can be obtained as follows:

$$N_f = \frac{(\beta+1)\left(S_{max}^{\beta+1} - S_{min}^{\beta+1}\right)^{-1}}{2B(\beta+2)} \tag{7}$$

$$D = 1 - \left(1 - \frac{N}{N_f}\right)^{1/(\beta+2)} \tag{8}$$

The material constant β can be obtained by fitted formula $S = 2407.41N^{-0.1555}$ from the fatigue tests of the MCX series samples, with β = 5.43. By inserting the value of β
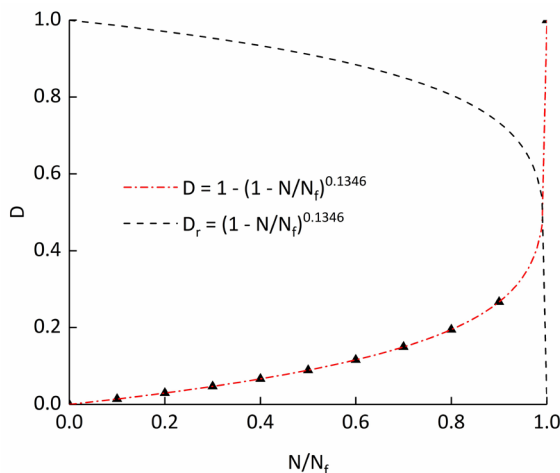

Figure 7. Fatigue damage curve.

into Equation 8, the fatigue damage curve of MCX series samples was shown in Figure 7.

Figure 7 shows a residual life analysis model based on Miner's linear cumulative damage correlation theory. When $N/N_f < 0.9$, damage variable D varied linearly following the increment of recycle ratio. When $N/N_f > 0.9$, the specimen entered the transient fracture stage, damage variable D increased rapidly to 1 following the recycle ratio, and the specimen underwent a large amount of plastic damage, from which it could not recover. When $N/N_f = 0.9$, the damage variable D of the MCX specimen before fracture was about 0.27. The MCX-6 specimen was subjected to cyclic loading at a stress of 237.19 MPa. By substituting s = 237.19 MPa into the fitting formula $S = 2407.41N^{-0.1555}$, $N_F = 2,967,364$ was obtained. The testing was not stopped for two million stress cycles, at which point, d = 0.14. Then, the MCX-6 sample was modified to the MCD-4* sample, and the load–displacement relationship obtained from the monotonic tensile test is presented in Figure 2. Static tensile strength and deformation of the MCD-4* specimen were not affected by the previous fatigue loading, following the experimental results of the MCD-4* sample, and the plastic damage was neglected when d = 0.14.

4. Evaluation of Fatigue Characteristics of Q420C Steel

4.1. Comparison with current standards

The British standard BS7608:2014 + A1:2015[23], is a standard for the fatigue strength analyses, prediction of fatigue life and assessment of a base metal and various welded joints with yield strengths of 200~960 MPa. For all kinds of base metal and its connections that meet the requirements, the amplitude of stress change S_r and times of repeated loading N contented the Formula 9:

$$\log N = \log C_0 - dSD - m\log S_r \tag{9}$$

Where N is cycle number of the cyclic loading, S_r is the amplitude of stress change, C_0 is sample parameter defining the Miner's linear S_r-N regular, m is the inverse slope of the $\log S_r$-$\log N$ curve, SD is sample standard deviation of the random variable logN, and d is the standard deviations coefficient of logN and Miner's S_r-N curves corresponding to a specific guarantee rate. For the Q420C steel plate with 8-mm thickness, where $C_0 = 1.082 \times 10^{14}$, m = 3.5, SD = 0.2041, the nominal failure probability is 50%, and d = 0, the equivalent transformations of Formula 9 are as follows:

$$S_r = 10227.73N^{-(1/3.5)} \tag{10a}$$

$$\log S_r = 4.01 - 0.2857\log N \tag{10b}$$

In the GB50017-2017 Steel Structure Design Standard[24], the permissible stress design means was adopted in member and join fatigue design. The permissible stress range [Δσ] depended on the type of member or join, times of repeated loading, and parent metal plate thickness at the calculated position. The following formulas are used for fatigue checking of the base metal:

$$\Delta\sigma \leq \gamma_t\left[\Delta\sigma\right] \tag{11}$$

$$\left[\Delta\sigma\right] = \left(C_z/N\right)^{1/\beta_z} \tag{12}$$

where γ_t is the plate thickness correction factor, C_z and β_z are parameters of the component and the connection type, respectively, and N is cycle number of the cyclic loading. For the 8-mm Q420C steel plate, $\gamma_t = 1.0$, $C_z = 861 \times 1012$, $\beta_z = 4$, and $\Delta\sigma = \sigma_{max} - 0.7\sigma_{min}$. The equivalent transformations of Formula 11 are as follows:

$$S = 5416.92N^{-0.25} \tag{13a}$$

$$logS = 3.734 - 0.25logN \tag{13b}$$

The formula for calculating the base metal fatigue properties of ANSI/AISC360-10 is as follows (14) :

$$F_{SR} = \left(\frac{C_f \times 329}{N}\right)^{0.333} \geq F_{TH} \tag{14}$$

where F_{SR} is the permitted stress range, N is cycle number of the cyclic loading, C_f is the fatigue type coefficient, and F_{TH} is the critical permitted stress range. In this paper, Q420C steel samples are transformed by an equivalent transformation with $C_f = 250 \times 10^8$, $F_{TH} = 165$ MPa, and

Figure 8. Comparison between test fitted and standard S-N curve.

$F_{SR} = S_{max} - 0.7S_{min}$. The equivalent transformations of Formula 14 are as follows:

$$S = 19986.7N^{-0.333} \tag{15a}$$

$$logS = 4.3007 - 0.33logN \tag{15b}$$

The fitted S–N curve for Q420C steel is compared with the standard S-N curve in Figure 8. The fitted curve and 95% guarantee curve of the MCX series were much more than those of BS7608:2014, GB50017-2017, and ANSI/AISC360-10. The 95% fatigue limit for N = 2 × 10⁶ stress cycles was 1.4 times that of BS7608:2014, 1.58 times that of GB50017-2017, and 1.43 times that of ANSI/AISC360-10. The values of the BS7608:2014 S-N curve were close to those of the ANSI/AISC360-10 S-N curve, and the values of the GB50017-2017 S-N curve were the most conservative. Overall, the values of the fatigue properties of Q420C steel were much higher than those of the standard formula, which showed that the S-N curve formula provided by the standard is conservative for Q420C steel.

4.2. Comparison of fatigue properties of steel with different strength grades

Many fatigue tests have been carried out for various strength grades of steel, but the analysis and comparison of the fatigue properties of different strength grades of steel are still lacking. In order to better understand the fatigue properties of steel, the fatigue test results from existing literature were compared with those of the Q420C steel in this paper. The loading parameters of the fatigue test usually include frequency, the maximum load, minimum load, target setpoint, amplitude, and wave shape. The fatigue test conditions of previous studies are presented in Table 5. The logarithmic linear relationship between the stress level and the fatigue life is usually obtained using the least squares method during test data processing, which is equivalent to the commonly used power function form. The S-N curves of various kinds of steels are shown in Table 6 and Figure 9. The stress level S in the S-N curve represents S_{max} in some previous reports, but S represents the stress range in this study.

The comparison between the equations in Table 6 and the S-N curves in Figure 9 showed the following:

(1) Overall, the higher the steel strength grade was, the higher the S-N curve was, that is, the fatigue strength was related to the strength grade of the steel. The higher the material strength was, the greater the fatigue strength was.
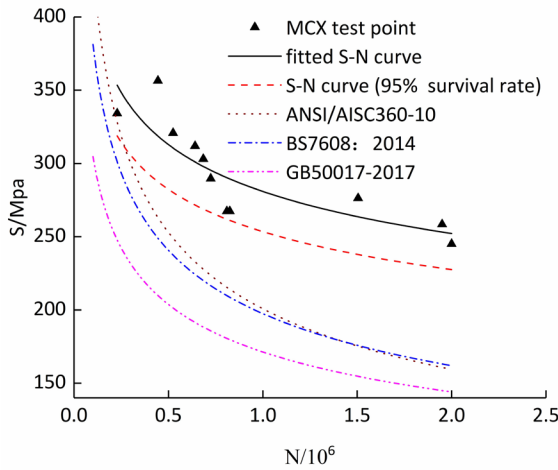
Table 5. Loading parameters and test conditions of steel fatigue test.

| Data source	Steel grade	f_y/MPa	f_u/MPa	Stress ratio	t/mm	f/Hz	Load waveform
Ref. [2]	Q390GJD-16	392.0	565.0	0.1	16	100	Sine wave
Ref. [3]	Q460C-14	492.27	631.23	0.1	14	100	Sine wave
Ref. [4]	Q460D-14	465	560	0.1	14	100	Sine wave
Ref. [7]	Q460D-8	504.9	592.0	0.1	8	30	Sine wave
Ref. [8]	Q690D-8	786.3	832.0	0.1	8	20/25	Sine wave
Ref. [25]	Q690D-8*	733.0	815.25	0.1	8	30	Sine wave
Ref. [5]	Q690D-10	800.0	840.0	0.1	10	15/20	Triangular wave
This paper	Q420C-8	478.3	546.7	0.1	8	15	Sine wave
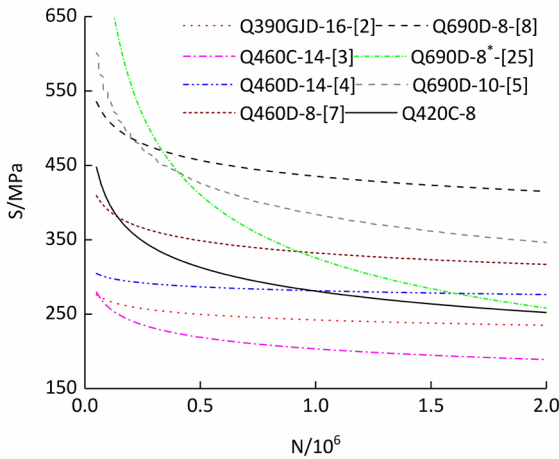
Figure 9. S-N curves from fatigue tests of steel.

Table 6. Fitted S-N curve equations of steel in fatigue tests.

Type of steel	Relationship of S_{max}-N	Relationship of S-N
Q390GJD-16	$S_{max} = 478.366N^{-0.044}$	$S = 444.88N^{-0.044}$
Q460C-14	$S_{max} = 948.593N^{-0.10622}$	$S = 882.19N^{-0.10622}$
Q460D-14	$S_{max} = 436.275N^{-0.02647}$	$S = 405.73N^{-0.02647}$
Q460D-8	$S_{max} = 933.66N^{-0.06950}$	$S = 868.3N^{-0.06950}$
Q690D-8	$S_{max} = 1216.35N^{-0.0691}$	$S = 1131.2N^{-0.0691}$
Q690D-8*	$S_{max} = 35776.68N^{-0.3349}$	$S = 33272.31N^{-0.3349}$
Q690D-10	$S_{max} = 3255.367N^{-0.14941}$	$S = 3027.49N^{-0.14941}$
Q420C-8	$S_{max} = 2588.6N^{-0.1555}$	$S = 2407.41N^{-0.1555}$

(2) Q460C and Q460D steels have the same strength grade; yet, the impact toughness of Q460D was better than that of Q460C, and the fatigue curve was also above that of Q460C. This showed that the high fatigue strength of the quality grade was high. The curve of Q390GJD was between the curves of Q460C-14 and Q460D-14, and this was also related to the quality grade.

(3) According to the fatigue curves of Q460D-8 and Q460D-14, the thickness of the steel plate had a significant effect on the fatigue properties. The initial defects in the steel plate increase and the fatigue properties becomes worse, because of the increase at the steel plate thickness. The quantitative effect of the thickness on the fatigue properties of the base metal are not presented in many of the standards. In GB50017-2017, γ_t is introduced to account for the effect of the plate thickness on the fatigue strength of bolted or welded connections. The quantitative effects of plate thickness and environmental changes on fatigue strength of various grades of steel need to be studied systematically.

(4) The three fitted fatigue curves of Q690D steel were different, which indicated that the data of the fatigue tests were significantly different. This may have been caused by the different qualities of the different batches of steel.

(5) The fitting results of the fatigue tests of Q420C steel were basically consistent with the findings discussed above, which showed that the experimental study of this paper was reasonable. Because of the discreteness, it is necessary to increase the influence of various geometric dimensions, such as the thickness of the plate, to determine the quantitative influence of the geometric dimensions. It is also necessary to consider the effect of the working conditions, such as environmental changes, on the fatigue performance.

5. Conclusions

The fatigue strength S-N curve of Q420C steel have been studied in this paper. Data were obtained from an experimental study on the high-cycle fatigue properties of Q420C steel plates with 8-mm thicknesses at room temperature. In addition, the fatigue properties of Q420C steel were comprehensively evaluated by comparison with the S-N curves of various standards and steels of other strength grades. The following conclusions were drawn:

(1) After the high-cycle fatigue test, the failure of the smples were typical fatigue failure, except the unbroken ones. The fracture surface was primary composed of the extended region and instantaneous fracture region. There are clear bands of fatigue cracks in the extended region.

(2) The values of the fitted curves and the 95% guarantee rate were much larger than the corresponding values of the BS7608:2014, GB50017-2017, and ANSI/AISC360-10 standard curves. The formula for the S-N curve stipulated in the standard is conservative for Q420C steel. Consideration should be given to raising the standard value appropriately.

(3) Under the action of extreme stress, the corresponding displacement is divided into three stages, and the change of the displacement value reflects the fatigue failure course of the materials. The fatigue test results of Q420C steel were in good agreement with the residual life model based on Miner's linear cumulative damage theory.

(4) According to the steel fatigue curves, the thickness of the steel plate had a significant effect on the fatigue properties. The initial defects in the steel plate increase and the fatigue performance becomes worse, because of the increase at the steel plate thickness. The quantitative effects of plate thickness and environmental changes on fatigue strength of Q420C steel need to be studied systematically.

6. Acknowledgments

7. References

1. Li ZR, Zhang DC, Wu HY, Huang FH, Hong W, Zang XS. Fatigue properties of welded Q420 high strength steel at room and low temperatures. Constr Build Mater. 2018;189:955-66.

2. Shi G, Zhang JX, Wang Z, Song WJ. Fatigue test of structural steel Q390GJD. Steel Construction. 2014;29(8):21-6. [Chinese]

3. Shi G, Zhang JX. Fatigue Performance test study on high strength steel Q460C and its welded connection. Building Structure. 2014;44(17):1-6. [Chinese]

4. Shi G, Zhang JX. Fatigue test of high strength steel Q460D. Industrial Construction. 2014;44(3):6-10. [Chinese]

5. Kang L, Hong ST. Experimental investigation on fatigue properties of Q690D high strength steel. Journal of South China University of Technology [Natural Science Edition]. 2021;49(8):35-42.

6. Tong LW, Niu LC, Ren ZZ, Zhao XL. Experimental research on fatigue performance of high-strength structural steel series. J Construct Steel Res. 2021;183:1-15.

7. Guo HC, Hao LP, Li YL, Liu YH, Wan JH. Experimental study on fatigue Performance of Q460D high-strength steel and its welded joints. Journal of Building Structures. 2018;39(8):157-64. [Chinese]

8. Guo HC, Wan JH, Liu YH, Wang DF. Experimental study on fatigue Performance of Q690D high strength steel welded joints. Tumu Gongcheng Xuebao. 2018;51(9):1-9. [Chinese]

9. Guo HC, Wan JH, Liu YH. Experimental study on fatigue performance of high strength steel welded joints. Thin-walled Struct. 2018;131:45-54.

10. Guo HC, Mao KH, Wan JH, Hao JP, Li S, Wang ZS. Research progress on fatigue properties of high strength steels. Journal of Building Structures. 2019;40(4):17-28. [Chinese]

11. Fan JL. High cycle fatigue behavior evaluation of Q235 steel based on energy dissipation. Journal of Mechanical Engineering. 2018;54(6):1-9. [Chinese]

12. Liu HQ, Huang ZY, Wang QY. Study on high cycle fatigue failure mechanism and intrinsic dissipation energy investigations of Q345. Advanced Engineering Sciences. 2017;49(6):157-62.

13. Liu HQ, Wang QY, Huang ZY, Teng ZJ. High-cycle fatigue and thermal dissipation investigations for low carbon steel Q345. Key Eng Mater. 2016;664:305-13.

14. Cicero S, García T, Álvarez JA, Martín-Meizoso A, Bannister A, Klimpel A. Definition of BS7608 fatigue classes for structural steels with thermally cut edges. J Construct Steel Res. 2016;120:221-31.

15. Zhang DC, Li ZR, Wu HY, Huang F. Experimental study on fatigue behavior of 420 high-strength steel at low temperatures. J Construct Steel Res. 2018;145:116-27.

16. China Standard Press. GB/T1591-2008: High strength Low alloy structural steels. Beijing: China Standard Press; 2009. [Chinese]

17. China Standard Press. GB/T228.1-2010: Metallic materials-Tensil testing-Part 1: Method of test at room temparsture. Beijing: China Standard Press; 2011. [Chinese]

18. Yao WX. Fatigue life estimation of structures. Beijing: National Defense Industry Press; 2019. [Chinese]

19. Chen SF. Principle of steel structure design. Beijing: Science Press; 2005. [Chinese]

20. China Standard Press. GB/T3075-2008: Metallic materials-fatigue testing-axial force controlled method. Beijing: China Standard Press; 2008. [Chinese]

21. AISC: American Institute of Steel Construction. ANSI/AISC360-10: specification for structural steel buildings. Chicago: AISC; 2010.

22. Lou ZW. Damage mechanics foundation. Xi'an Shaanxi Province: Xi'an Jiaotong University Press; 1991. [Chinese].

23. BSI: British Standards Institution. Guide to fatigue design and assessment of steel products: BS7608-2014. London: BSI; 2014.

24. China Standard Press. Standard for design of steel Structures: GB50017-2017. Beijing: Planning Press; 2017. [Chinese]

25. Guo HC, Wei HH, Yang DX, Liu YH, Wang ZS, Tian JB. Experimental research on fatigue performance of Q690 high strength steel in marine corrosive environment. Tumu Gongcheng Xuebao. 2021;54(5):36-45. [Chinese]